A peer-reviewed version of this preprint was published in PeerJ on 30 April 2018.

View the peer-reviewed version (peerj.com/articles/4656), which is the preferred citable publication unless you specifically need to cite this preprint.

Silva MdA, Leite YKdC, Carvalho CESd, Feitosa MLT, Alves MMdM, Carvalho FAdA, Neto BCV, Miglino MA, Jozala AF, Carvalho MAMd. 2018. Behavior and biocompatibility of rabbit bone marrow mesenchymal stem cells with bacterial cellulose membrane. PeerJ 6:e4656
https://doi.org/10.7717/peerj.4656

PeerJ Preprints NOT PEER-REVIEWED

Behavior and Biocompatibility of rabbits bone marrow Mesenchymal Stem Cells with bacterial cellulosic membrane

Marcello A. Silva[1]; Yulla K. Carvalho[1]; Camila E. Carvalho[2]; Matheus L. Feitosa[2]; Fernando A. Carvalho[3], Bartolomeu C.Viana [4,5] Maria Angélica Miglino[6], Ângela F. Jozala[7]; Maria Acelina M. Carvalho[1,2]

[1] Biotechnology Graduate Program, Integrated Nucleus of Morphology and Stem Cell Research, Federal University of Piauí, Teresina, Piauí, Brazil.

[2] Animal Science Graduate Program, Federal University of Piauí, Teresina, Piauí, Brazil.

[3] Antileishmania Activities Laboratory, Federal University of Piauí, Teresina, Piauí, Brazil.

[4] Advanced Microscopy Multiuser Laboratory, Federal University of Piauí, Teresina, Piauí, Brazil.

[5] Department of Physics, Laboratory of Physics Material, Federal University of Piauí, Teresina, Piauí, Brazil.

[6] Department of surgery. Faculty of Veterinary Medicine and Animal Science - USP, São Paulo, Brazil.

[7] Laboratory of Toxicological Research, University of Sorocaba - UNISO, Sorocaba, São Paulo, Brazil.

Corresponding Author:

Marcello A. Silva[1]

Email address: dr.marcelloalencar@outlook.com

Maria Acelina M. Carvalho[1,2]

Email address: mcelina@ufpi.edu.br

Background. Tissue engineering has been shown to exhibit great potential for the creation of biomaterials capable of developing into functional tissues. Cellular expansion and integration depends on the quality and surface-determinant factors of the scaffold, which are required for successful biological implants. The objective of this research was to characterize and evaluate the *in vitro* characteristics of rabbit bone marrow mesenchymal stem cells (BM-MSCs) associated with a bacterial cellulose membrane (BCM). We assessed the adhesion, expansion, and integration of the biomaterial as well as its ability to induce macrophage activation. Finally, we evaluated the cytotoxicity and toxicity of the BCM.

Methods. Samples of rabbit bone marrow were collected. Mesenchymal stem cells were isolated from medullary aspirates to establish fibroblast colony-forming unit assays. Osteogenic, chondrogenic, and adipogenic differentiation was performed. Integration with the BCM was assessed by scanning electron microscopy at 1, 7, and 14 days. Cytotoxicity was assessed via the production of nitric oxide, and BCM toxicity was assessed with the MTT assay; phagocytic activity was also determined.

Results. The fibroblastoid colony-forming unit (CFU-F) assay showed cells with a fibroblastoid morphology organized into colonies, and distributed across the culture area surface. In the growth curve, two distinct phases, lag and log phase, were observed at 15 days. Multipotentiality of the cells was evident after induction of osteogenic, chondrogenic, and adipogenic lineages. Regarding the BM-MSCs' bioelectrical integration with the BCM, BM-MSCs were anchored in the BCM in the first 24 h. On day 7 of culture, the cytoplasm was scattered, and on day 14, the cells were fully integrated with the biomaterial. We also observed significant macrophage activation; analysis of the MTT assay and the concentration of nitric oxide revealed no cytotoxicity of the biomaterial.

Conclusion. The BCM allowed the expansion and biointegration of bone marrow progenitor cells with a stable cytotoxic profile, thus presenting itself as a biomaterial with potential for tissue engineering.

Subjects: Biotechnology, Cell Biology, Engineering Tissue, Translational Medicine.

Key-words: Stem Cells; Tissue Engineering; Culture Techniques; Biocompatible Materials; Cellulose.

Introduction

Researchers have been studying bone marrow mesenchymal stem cells (BM-MSCs) for their applicability in regenerative medicine, and for improving current methodologies (Dimarino, Caplan & Bonfield, 2013; Wei et al., 2013; Kobolak et al., 2016; Li et al., 2016). BM-MSCs are widely used in clinical and therapeutic use due to several factors: they are easily accessible; it is possible to achieve the necessary volume of cells in a short time, through culture replication; they allow autologous use or the treatment of several patients with a single sample, since the expression of HLA antigens is poor; they can be used without the need for HLA typing, making them ready for use in any patient. Even after being frozen, they preserve their characteristics, which allows the creation of bio-banks (Wabik & Jones, 2015).

The use of mesenchymal stem cells (MSCs) has shown promise in the field of regenerative medicine. Studies have investigated the use of MSCs in cardiovascular events (Castellanos et al., 2016), immunological dysfunctions (Kaplan, Youd & Lodie, 2011; Zao, Ren & Han, 2016), bone repair (Emmet et al., 2016), cartilaginous and intervertebral discs (Blanquer, Grijpma & Poot, 2015), tendinosis (Peach et al., 2017), and hematological malignancies (Wang, Qu & Zhao, 2012), among others (Schnitzler et al., 2016; Squillaro, Peluso & Galderisi, 2016). Tissue engineering is a promising multidisciplinary field that involves the development of materials or devices capable of specific interactions within biological tissues (Langer & Vacanti, 2016). Advances in research have demonstrated biocompatibility between stem cells and biopolymers in the development of *in vitro* tissues capable of repairing injured areas (Lima et al., 2017; Park et al., 2017; Weinstein-Oppenheimer et al., 2017).

Several biomaterials with different physicochemical and mechanical properties have been developed, with biomedical purposes including tissue regeneration, drug delivery systems, new vascular grafts, or *in vitro* and *in vivo* tissue engineering supports (Lin, Lien & Yeh, 2013; Yan et al., 2013; Soheilmoghaddam, Sharifzadeh & Pour, 2014; Zulkifli, Hussain & Rasad, 2014; Kim & Kim, 2015; Pires, Bierhalz & Moraes, 2015; Urbina, Algar & García-Astrain, 2016).

The scaffold surface can generate cellular responses which can affect adhesion, proliferation, migration, biointegration, and cellular function (Abbott & Kaplan, 2016). This interaction is especially important to define the degree of rejection of medical implants (Achatz et al., 2016).

Bacterial cellulose is an extracellular polysaccharide secreted primarily by *Gluconacetobacter xylinus*, an aerobic, Gram-negative, and chemoheterotrophic bacterium that can be grown in liquid medium from various sources of carbon and nitrogen, and basically uses glucose as the substrate. In culture medium, this microorganism produces very fine fibers that intertwine, forming a film with a nanofibrillar structure (Moosavi-Nasab & Yousefi, 2011; Li et al., 2012; Panesar et al., 2012). Nanofibrils of length from 20 to 100 nm intertwine, forming a three-dimensional network, resulting in a high degree of hydrophilicity (Jozala et al., 2015; Rajwade et al., 2015), water retention capacity, and porosity, which allows selective permeability, adhesion of cell culture, and diffusion of the culture medium (Cavka et al., 2013; Vieira, 2013; Ashok et al., 2015; Kirdponpattara et al., 2015).

96 Many studies have used the bacterial cell membrane *in vitro*, in preclinical studies
97 investigating drug, hormone, and protein release systems, artificial skin (Fu, Zhang & Yang,
98 2013), cartilage (Cruz, Severo & Azzolin, 2016), menisci (Achatz, Kuat & Pfeifer, 2016),
99 intervertebral discs (Flávaro, Arruda & Vialle, 2016), valvular prostheses, artificial corneas, and
100 the urethra (Rajwade, Paknikar & Kumbhar, 2015). However, it will be necessary to improve our
101 knowledge of bacterial cellulosic membrane (BCM) biointegration and biodegradation, especially
102 with respect to BM-MSCs.
103 This purpose of this study was to characterize and evaluate rabbit BM-MSC behavior *in*
104 *vitro* when associated with a BCM, by analyzing adhesion, expansion, and cellular integration
105 with the biomaterial, as well as the ability to induce macrophage activation. BCM cytotoxicity
106 and toxicity were also evaluated.
107

108 **Material and Methods**

109 **Study design**

110 Samples of rabbit adult bone marrow were collected. MSC bone marrow was used for
111 isolation and cryopreservation. A *Mus musculus* mouse was used as a source of peritoneal
112 macrophages. To determine cellular viability, Trypan Blue staining and growth curve analysis
113 were performed. For the fibroblastoid colony-forming unit assay, cells collected from the bone
114 marrow (BM) cultured in 24-well plates at passage 6 were used. Chondrogenic, osteogenic, and
115 adipogenic induction were used to assess the potential for differentiation into mesenchymal
116 lineages. To verify BM-MSC biointegration with the BCM, inverted light microscopy and
117 scanning electron microscopy (SEM) were used to analyze the phagocytic capacity, toxicity, and
118 cytotoxicity of the BCM. This study was performed in strict accordance with the
119 recommendations of the Guide for the Care and Use of Laboratory Animals of the National
120 Institutes of Health. The protocol was approved by the Ethics Committee on the Use of Animals
121 of the Federal University of Piauí (permit number: 268/16).
122

123 **Anesthetic protocol for bone marrow collection**

124 After solid anesthetic fasting of 4 h, and 2 h of liquids, the rabbit was chemically restrained
125 with a combination of 35 mg/kg of ketamine hydrochloride and 3 mg/kg of midazolam maleate.
126 Trichotomy of the major trochanter region was performed, followed by antisepsis by femoral

127 puncture with a 5 mL syringe; a heparinized 40 × 12 mm needle was used to obtain a BM sample.
128 For antibacterial prophylaxis, 10 mg/kg of enrofloxacin was given twice daily for 7 days, and 25
129 mg/kg of sodium dipyrone plus 3 mg/kg of tramadol was administered twice daily for 3 days for
130 pain control.
131
132 **BM-MSC isolation, cultivation, and expansion**
133 Medullary aspirate (1.5 mL) was diluted in phosphate-buffered saline (PBS) at a ratio of
134 1:1 in 15 mL conical tubes. The resulting contents were filtered through 100 µm mesh, deposited
135 in a 15 mL conical tube containing Ficoll Histopaque at a ratio of 1:1 (Ficoll:BM), and
136 centrifuged at 2,000 rpm for 30 min at 20 °C to separate the cellular constituents by density
137 gradient. The whitish halo, rich in mononuclear cells, was aspirated with an automatic pipettor
138 (Houston), immediately diluted in sterile PBS with 1% antibiotic (100 U/mL penicillin and 100 µg/mL
139 streptomycin) for cell lavage, and re-centrifuged at 1,500 rpm for 10 min at 20 °C. BM samples were
140 resuspended in complete Dulbecco's modified Eagle's medium (DMEM) containing 3.7 g/L sodium
141 bicarbonate and 10–15 mM HEPES (Invitrogen, no. 15630080), pH 7.5, 15% fetal bovine serum
142 (Invitrogen), 1% penicillin–streptomycin, 1% L-glutamine (Invitrogen), and 1% non-essential amino acids
143 (Sigma), and cell viability was assessed. For this purpose, a 50 µL aliquot of each sample was diluted in 50
144 µL 0.2% Trypan Blue dye, and mixed in a sterilized glass vial for cell counting in a Neubauer chamber
145 (Argôlo Neto et al., 2016).
146 Cells were seeded in a six-well cell culture plate (TPP) at a density of 10^6 cells/well in 2.0
147 mL of low-glucose DMEM, and kept in an incubator (Thermo Scientific Series II Water Jacket)
148 at 37 °C in 5% CO_2 and 95% humidity. The wells were washed twice every 3 days with PBS
149 solution containing 1% antibiotic (100 U/mL penicillin and 100 µg/mL streptomycin), followed
150 by exchange of the culture medium until the cultures reached 80% confluency. Subsequently, the
151 wells were subjected to trypsinization with 2.0 mL 1× trypsin (Invitrogen, no. 25200-114, 10×
152 Trypsin–EDTA solution), and incubated at 37 °C for 5 min. Following this, trypsin was
153 inactivated with the addition of 4.0 mL low-glucose DMEM. The solution was transferred to a 15
154 mL conical bottom tube, and centrifuged (FANEM refrigerated Cytocentrifuge MOD.280R
155 Excelsa 4) at 20 °C and 1,500 rpm for 10 min.
156 The supernatant was discarded, the pellet was resuspended in 1.0 mL of DMEM, and a new
157 cell count was performed. The cells in suspension were used for expansion. To do this, 10^6

158 cells/mL in 25 cm^2 tissue culture bottles with 3.0 mL of supplemented DMEM were incubated at
159 37 °C in 5% CO_2 and 95% humidity. The cultures were expanded and photographed with an
160 inverted phase-contrast microscope (COLEMAN NIB-100), and peaked with twice the original
161 area; cell concentration was verified at each passage.
162
163 **Cell viability**
164 Cell count, which determines concentration and viability, was performed using the Trypan
165 Blue exclusion method. After mixing 30 µL of the cell suspension with 30 µL Trypan Blue
166 solution (50 µL of 4.25% sodium chloride in 200 µL of Trypan Blue), a 10 µL aliquot was
167 observed in a Neubauer chamber under an optical microscope (10× objective). The BM-MSC
168 growth curve was performed in duplicate by plating 1×10^4 cells/mL in five six-well plates, and
169 counting two wells every 24 h over the course of 15 days. The culture medium of the plates was
170 changed every 3 days to maintain nutrient availability.
171
172 **Fibroblastoid colony-forming unit assay**
173 After plating 1×10^4 cells/mL of the BM-MSC rabbit fraction in 24-well plates, plates were
174 observed daily to monitor the establishment of colonies with more than 30 cells. Cells were then
175 fixed with 4% paraformaldehyde for 30 min, and stained with Giemsa for 10 min at room
176 temperature. Any excess stain was washed away with distilled water. The colonies were observed
177 and macroscopically counted on the 24-well plates.
178
179 **Cell differentiation**
180 Analysis of cell differentiation potential was performed with sixth-passage BM-MSCs
181 cryopreserved in liquid nitrogen for 12 months. They were thawed and grown in 25 cm^2 bottles
182 for cell expansion until 80% confluency was reached. Cultures were then trypsinized and seeded
183 at the concentration according to the manufacturer's instructions, for chondrogenic, osteogenic,
184 and adipogenic differentiation.
185 For chondrogenic differentiation, 3×10^5 cells per well were seeded in a 96-well plate.
186 After 48 h, formation of spheroid bodies was observed, and the culture medium was replaced
187 with that from a Stem Pro Chondrogenesis Differentiation Kit. Exchange of the medium was
188 performed every 3 days during a 21-day period. Analysis was performed with histological

189 sections stained with Alcian Blue.

190 For osteogenic differentiation, 6×10^4 cells were seeded in a 24-well plate. Initially, the
191 supplemented culture medium was removed and replaced with the osteogenic induction medium,
192 and changed every 3 days during a 21-day period. During this period, morphological
193 characteristics of the cells were evaluated. After osteogenic differentiation, cells were stained
194 with Alizarin Red, which identifies the calcium-rich extracellular matrix, and is characteristic of
195 the presence of osteoblasts. To do this, the cell monolayer was washed with PBS, and fixed with
196 10% alkaline phosphatase (AP) for 30 min at room temperature. The AP was then removed, the
197 cell monolayer was washed with distilled water, and Alizarin Red was added for 5 min.
198 Subsequently, the dye was removed, and five washes were performed with distilled water; the
199 calcium-rich extracellular matrix and the amount of calcium deposits were recorded with an
200 inverted light microscope.

201 For adipogenic differentiation, 2×10^4 cells per well were seeded in a 24-well plate, and
202 Stem Pro Adipogenesis Differentiation Kit induction medium was added once the cells reached
203 80% confluency. The culture medium was exchanged every 3 days over a period of 10 days.
204 Once differentiation occurred, the culture was stained with Oil Red to visualize lipid vacuoles.

205

206 **BM-MSC biointegration with the BCM**

207 To study BM-MSC expansion and biointegration with the BCM, 2×10^4 cells were cultured
208 in 12-well plates on BCM for three distinct periods (1, 7, and 14 days). The BM-MSCs were
209 fixed to the BCM using 3% glutaraldehyde, washed once with PBS, and dehydrated by slow
210 water exchange using a series of ethanol dilutions (30%, 55%, 70%, 88%, 96%, and 100%) for
211 20 min at each concentration. For analysis by SEM (FEI Quanta FEG 250), samples were fixed to
212 the stub with double-sided carbon tape, placed in a dehumidifier for 2 h, and metalized with gold.

213

214 **Phagocytic activation**

215 Phagocytic activity was assessed by collecting resident macrophages from the mouse
216 peritoneum. The animal was euthanized by cervical dislocation after being reassured and sedated
217 by intraperitoneal injection of a combination of xylazine hydrochloride and ketamine
218 hydrochloride (10 and 80 mg/kg body weight, respectively). Macrophage removal was performed
219 in a laminar flow hood with the animal affixed in the dorsal decubitus position by administering 8

220 mL of sterile PBS at 4 °C into the abdominal cavity. The abdominal region was softly massaged,
221 and aspiration was performed using a needle coupled to a sterile syringe. The cells were counted
222 in a Neubauer chamber by the Trypan Blue exclusion colorimetric method, and a minimum of
223 95% of living cells was obtained. The cells were counted using Neutral Red to obtain the desired
224 concentration of macrophages (2×10^5 cells/mL). Peritoneal macrophages were plated in each
225 well, and incubated on the BCM. After 48 h of incubation at 37 °C and 5% CO_2, 10 µL of stained
226 zymosan solution was added, and incubation continued for 30 min at 37 °C. Following this, 100
227 µL of Baker's fixative was added to paralyze the phagocytic process, and after 30 min the plate
228 was washed with 0.9% saline solution to remove the zymosan and Neutral Red that were not
229 phagocytized by macrophages. The supernatant was removed, 100 µL of extraction solution was
230 added, and after solubilization on a Kline shaker, absorbance was measured at 550 nm in a
231 BioTek plate reader (model ELx800) (Souza et al., 2017).
232
233 **Toxicity**
234 To assess toxicity, the nitric oxide (NO) induction test was performed. Peritoneal
235 macrophages (2×10^5 per well) were plated and incubated with the BCM after 24 h of incubation
236 at 37 °C and 5% CO_2. Cell supernatants were transferred to another 96-well plate for nitrite
237 dosing. The standard curve was prepared with sodium nitrite diluted in Milli-Q water at 1, 5, 10,
238 25, 50, 75, 100, and 150 µM in the appropriate culture medium. At the different timepoints, the
239 standard curve was determined with the same volume of Griess reagent (1% sulfanilamide in
240 10% H_3PO_4 [v:v] in Milli-Q water, added in equal parts to 0.1% naphthylenediamine in Milli-Q
241 water), and the absorbance was read on a BioTek plate reader (model ELx800) at 550 nm.
242 Lipopolysaccharide (LPS) was used as a positive control (Sundaram et al., 2016).
243
244 **BCM cytotoxicity**
245 The basis of cytotoxicity assays is the evaluation of biomaterial-induced interference in
246 cellular metabolic processes, and the investigation of processes that may intervene in cell
247 growth/multiplication, or even culminate in cell death (Ávila et al., 2014).
248 According to Boersema (2016), cytotoxicity can be evaluated by different methods
249 according to the type of cell damage: alterations in plasma membranes can be evaluated by means
250 of dyes such as Trypan Blue and alamarBlue; alterations in the metabolic functions of

251 mitochondria can be measured by the MTT (3-(4,5-dimethylthiazol-2-yl)-2,5-diphenyl
252 tetrazolium bromide) colorimetric method.

253 The experiments were performed separately in 24-well plates. In the first plate, 2×10^5
254 macrophages per well were plated, and 500 µL of supplemented RPMI 1640 medium was added.
255 In the second plate, 1×10^5 BM-MSCs in low-glucose DMEM were added. The plates were
256 incubated at 37 °C and 5% CO_2 for 4 h to allow for cell adhesion. Two washes were performed
257 with their respective media for removal of nonadherent cells. Subsequently, 500 µL of each
258 medium was added, and the BCM (diameter 15.4 mm) was added. Macrophages were incubated
259 for 48 h, and BM-MSCs for 7 days, followed by the addition of 10% 5 mg/mL MTT (diluted in
260 medium). The macrophages and BM-MSCs were incubated for another 4 h in an incubator at 37
261 °C with 5% CO_2. The supernatant was discarded, and 100 µL of dimethyl sulfoxide (DMSO) was
262 added to all wells. The BCM was removed, and the plate was shaken for 30 min on a Kline
263 shaker (model AK 0506) at room temperature for complete dissolution of the formazan. The
264 colorimetric reading was performed in a spectrophotometer at 550 nm in a BioTek plate reader
265 (model ELx800). In the control group, the same conditions were applied to the culture media and
266 the respective cultured cells (Barud et al., 2015).

267

268 **Statistical analysis**

269 For analysis of phagocytic capacity, Student's *t*-test was used for independent samples of
270 the cytotoxicity (MTT) and NO induction assays. GraphPad Prism version 5.0 was used to
271 generate the graphs. These tests were performed in triplicate.

272

273 **Results**

274 Immediately after isolation, cells from the BM appeared rounded and dispersed, and floated
275 in the culture medium. From the first day of culture, it was possible to identify undifferentiated
276 cells with a fibroblastoid morphology that had adhered to the plastic. On day 5, cells appeared to
277 still be in the adhesion process. On day 10, they were adhered and arranged in colonies with 80%
278 confluency in a 12-well plate (Fig. 1). After the first passage, cells reached confluency more
279 rapidly, with only a 5-day interval until 80% confluency was reached in 25 cm^2 bottles.

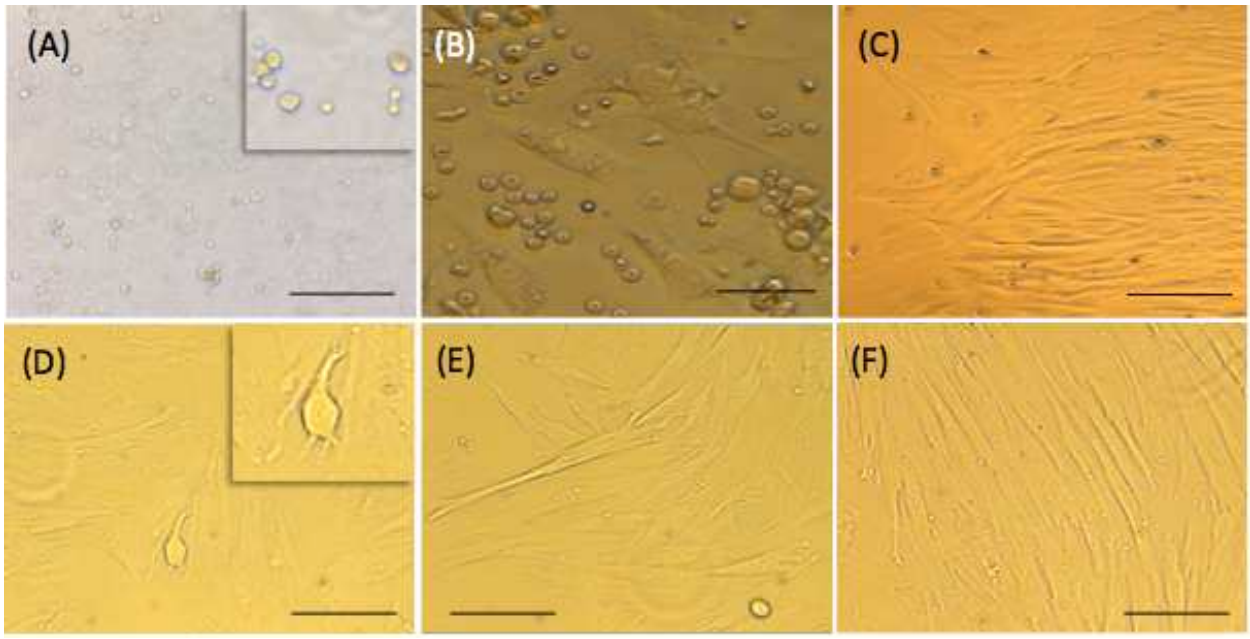

Figure 1. Bone marrow mesenchymal stem cell (BM-MSC) culture and expansion photomicrography. (A) Rabbit cells newly isolated from the bone marrow in 12-well plates (objective 4×, bar: 50 µm), (B) cells in the adhesion process on day 5 of cell culture performed in 12-well plates (objective 20×, bar: 25 µm), (C) cells arranged in parallel with fibroblastoid morphology at 80% confluency on day 10 of cell culture in 12-well plates (objective 10×, bar: 50 µm), (D) and (E) cytoplasmic adhesion and expansion with 80% confluency in 25 cm^2 bottles after trypsinization on day 15 of culture (objective 10×, bar: 50 µm), and (F) cells with fibroblastoid morphology arranged in parallel and in colonies at 80% confluency in 25 cm^2 bottles after trypsinization on day 20 of culture (10× objective, bar: 50 µm).

After thawing, cell cultures exhibited viability of 96%, with similar morphological characteristics and maintenance of differentiation as the primary culture. The observed time to confluency was superior to that of the first passage of the primary culture. At day 3, the culture showed 80% confluency. In the growth curve, we identified two phases (lag and log) which corresponded to the adaptation period of the cells to the culture conditions, the exponential growth period, and the stability period with a reduction in cell growth. Data regarding cell concentration were used to evaluate cell kinetics, and are presented in Fig. 2.

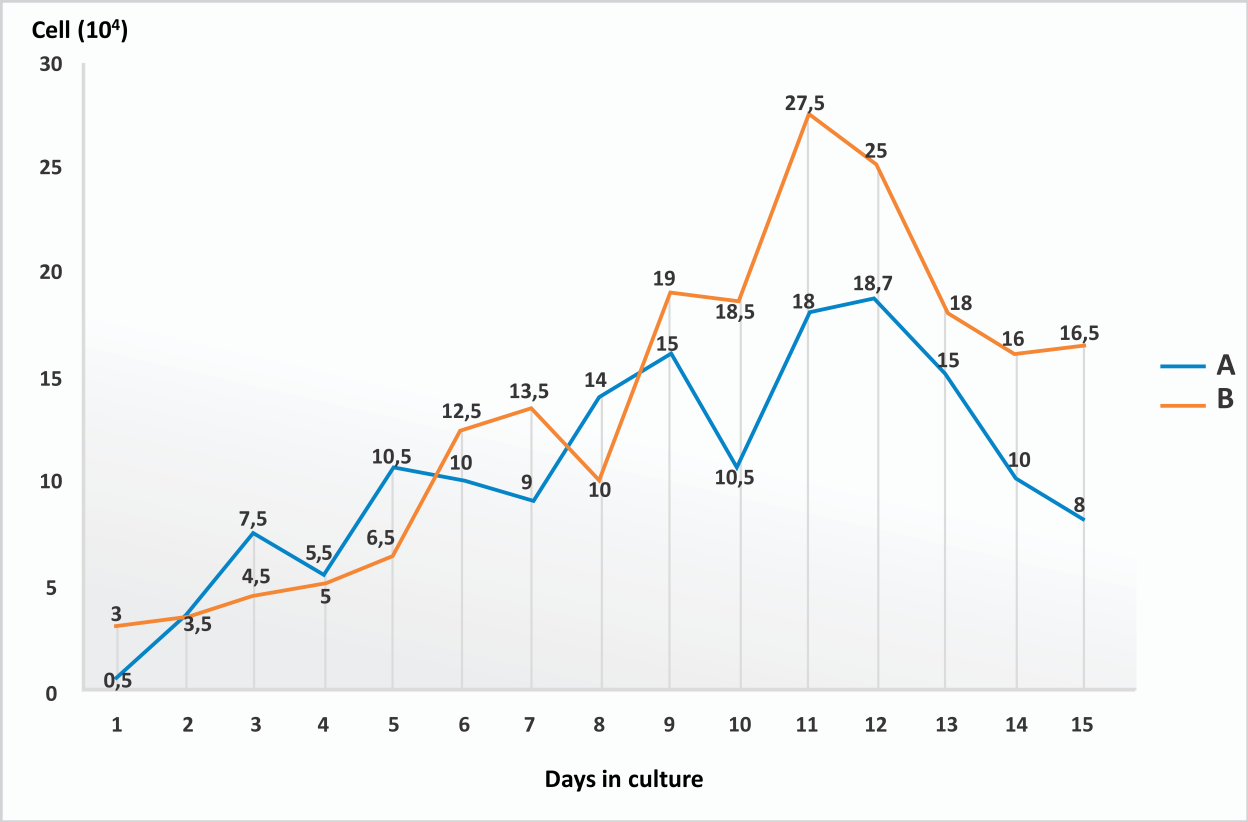

Figure 2. Growth curve of stem cells derived from rabbit bone marrow during 15 days of culture after thawing, at a concentration of 1×10^4 cells/mL. Phases identified: lag (days 1–4), log (days 5–11), and culture decline (days 12–15).

The formation and proliferation of fibroblast colonies were evident on day 2 of culture. Colonies were of varying sizes, surrounded by empty spaces, and distributed throughout the culture plate. The cells showed well-defined cytoplasmic boundaries, and nuclei with regions of condensed chromatin; the closer they were to one another, the more elongated the cells were, and they were arranged parallel to one another (Fig. 3).

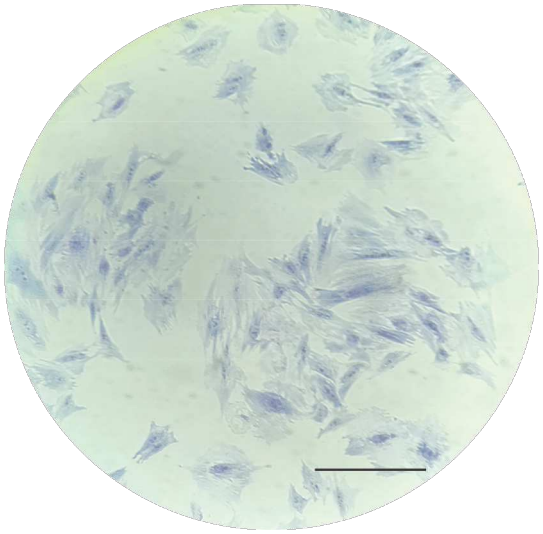

Figure 3. CFU-F assay in a 24-well plate: photomicrography of Giemsa-stained BM-MSC colonies after 2 days of cell culture at 80% confluency, and colonies with more than 30 cells per field (objective 20×, bar: 25 μm).

Differentiation into BM-MSC mesodermal lineages

The cell differentiation assay showed the potential of BM-MSCs to differentiate into chondrogenic and osteogenic lineages. Following chondrogenic differentiation, cells were stained vibrant blue by Alcian Blue, and control cells presented some spontaneous differentiation. Cells with fibroblastoid morphology adhered to the culture plate, and exhibited cytoplasmic integration (Fig. 4).

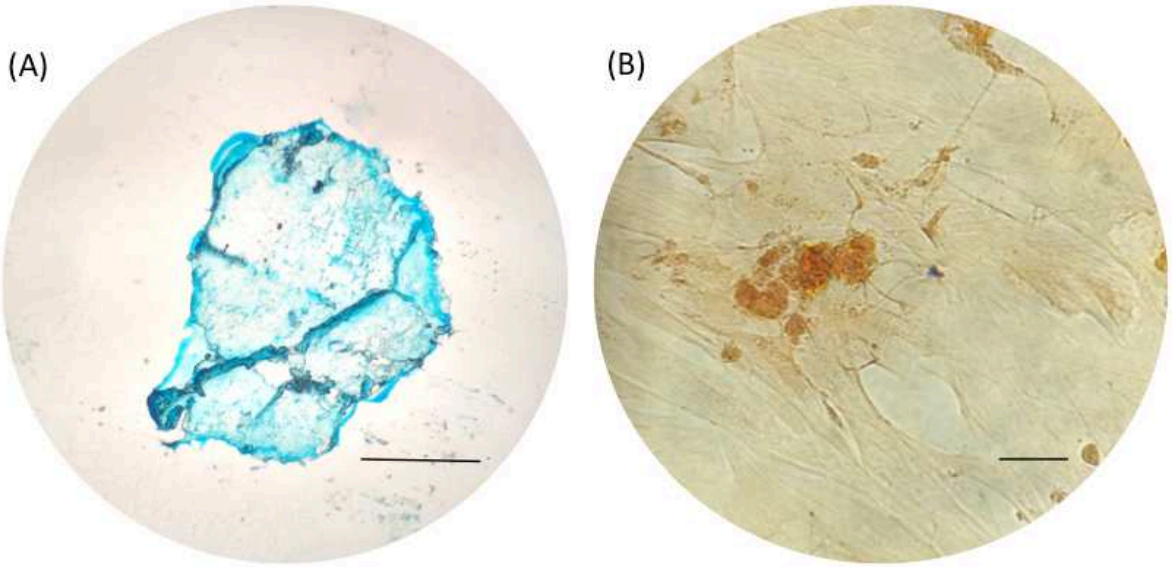

Figure 4. Photomicrographs showing BM-MSC differentiation. (A) BM-MSC chondrogenic differentiation (objective 20×, bar: 25 μm), and (B) negative control for 14 days of chondrogenic differentiation (objective 10×, bar: 25 μm).

321

322 During osteogenic induction, the culture demonstrated increased deposition of calcium in
323 the extracellular matrix from day 13 of culture. On day 21 of induction, the culture exhibited
324 osteogenic characteristics, which were confirmed with Alizarin Red staining (Fig. 5A). The
325 negative control showed adhered cells with morphology indicative of spontaneous differentiation
326 foci (Fig. 5B).

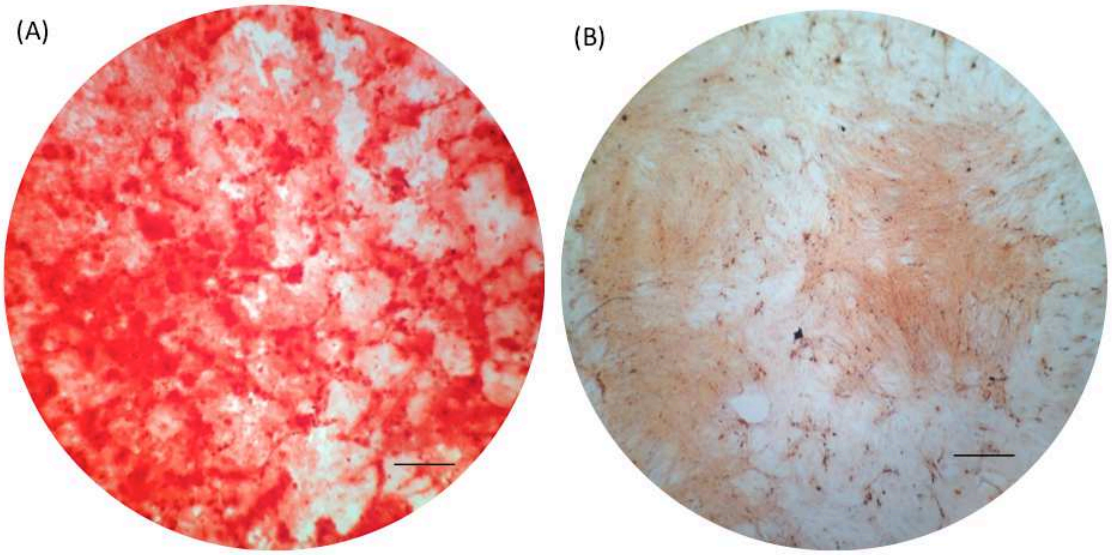

327

328 **Figure 5.** Photomicrographs showing BM-MSC differentiation. (A) BM-MSC osteogenic differentiation showing
329 calcium deposits in the extracellular matrix (objective 10×, bar: 25 μm), and (B) negative control for osteogenic
330 differentiation for 21 days (objective 10×, bar: 25 μm).

331

332 During adipogenic differentiation, the cells gradually changed to a fibroblastoid
333 morphology, and the cytoplasmic lipid vacuoles became bulky (Fig. 6).

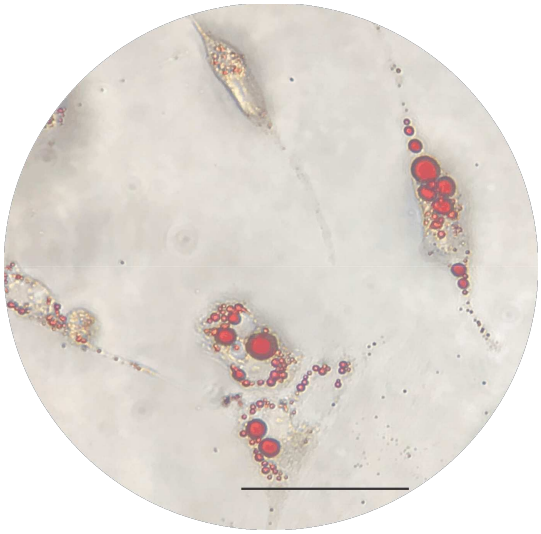

334

Figure 6. Photomicrograph showing the adipogenic differentiation of BM-MSCs, with lipid vacuoles present in the cytoplasm stained red with Oil Red (objective 40×, bar: 25 µm).

BM-MSC biointegration with the BCM

In the BCM-associated cell culture, BM-MSCs with a fibroblastoid shape integrated with the biomaterial, and proliferation of the colonies was evident at 14 days of culture (Fig. 7).

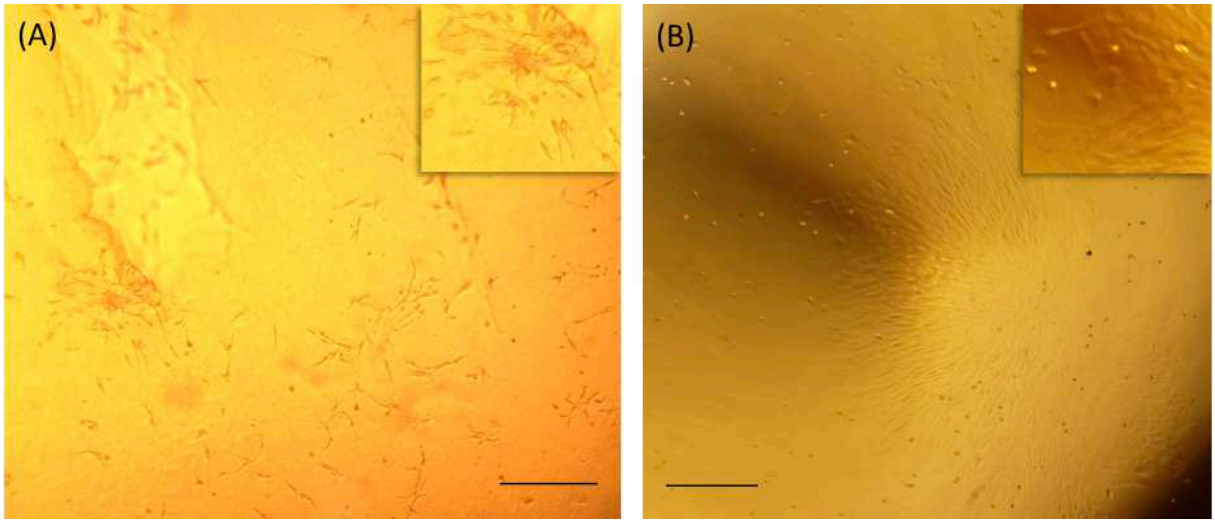

Figure 7. Photomicrographs of BM-MSCs adhered to the bacterial cellulosic membrane (BCM). (A) BM-MSC adhesion after 7 days of cell culture, highlighting the formation of CFU-F on the BCM (objective 20×, bar: 25 µm), and (B) BM-MSC colonies after 14 days of culture (objective 10×, bar: 50 µm).

Using SEM, it was possible to observe that the rounded shape of the cells after 24 h of culture was maintained after being subtly anchored to the randomly arranged fibers of the BCM. After 7 days of culture, the cells presented themselves in groups, forming colonies with several fixation points, generating greater adhesion to the biomaterial. Micrographs recorded after 14 days of cell culture show BM-MSCs with their cytoplasm fully integrated into the BCM (Fig. 8).

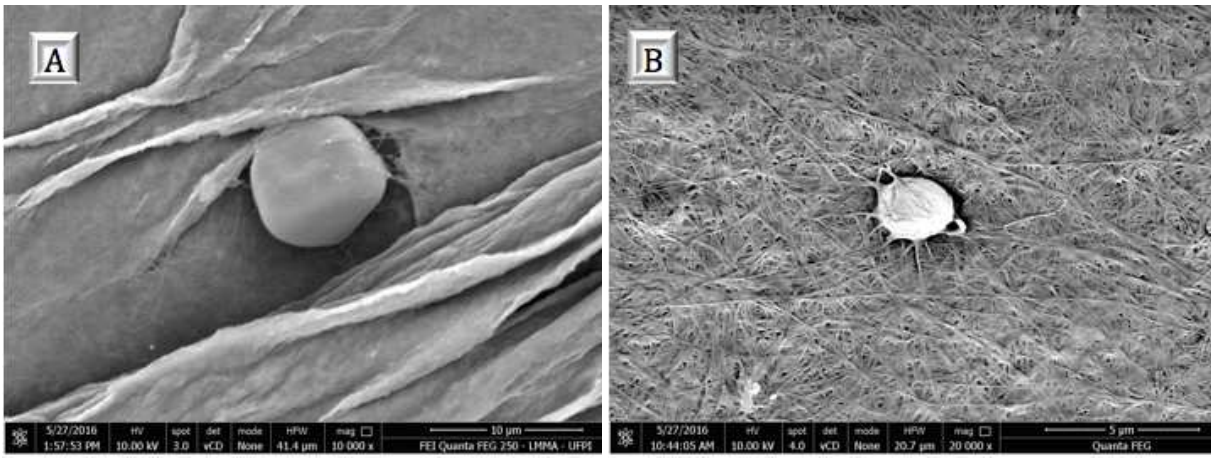

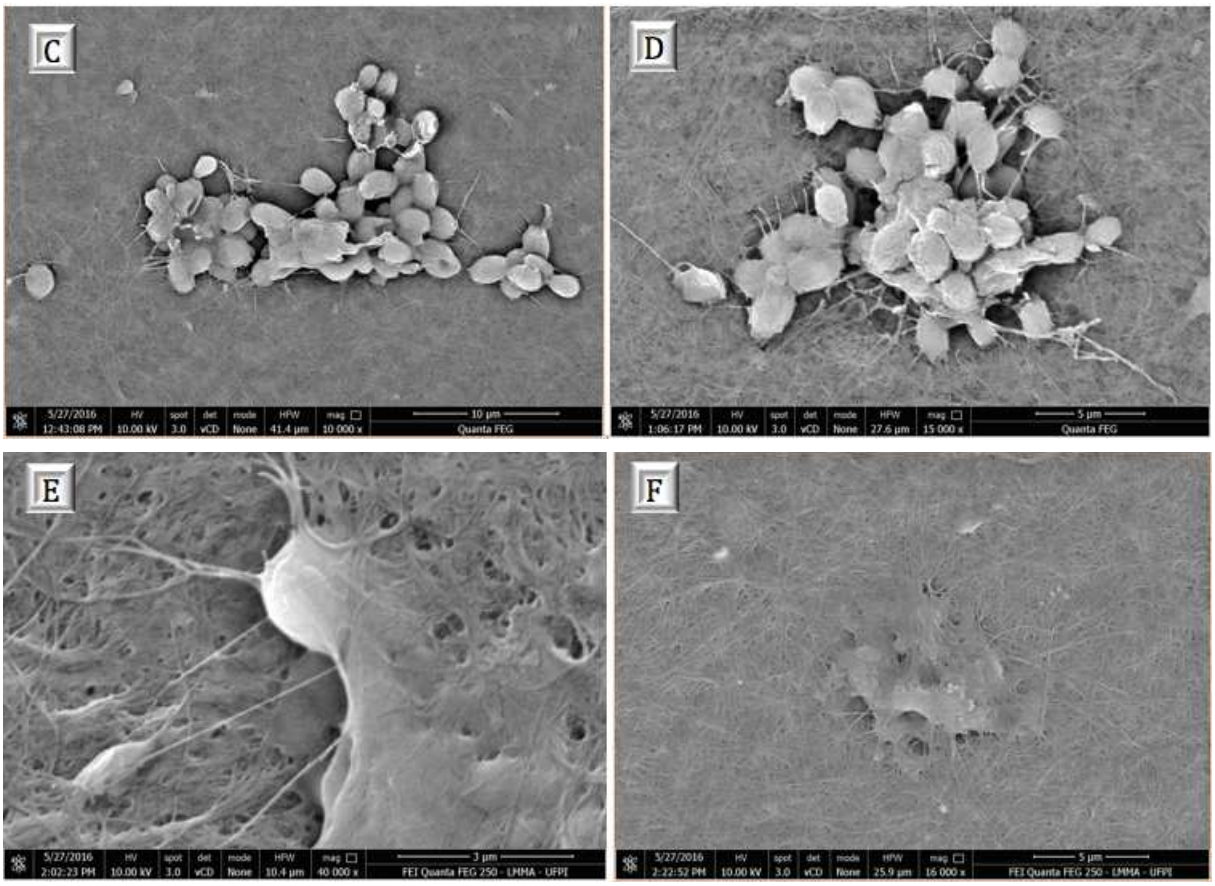

Figure 8. Scanning electron microscopy showing BM-MSC anchorage and biointegration with the BCM. (A) and (B) analysis after 24 h of cell culture (10,000× and 20,000×, respectively), and (C) and (D) with after 7 (E) and (F) 14 days of culture (40,000× and 16,000×, respectively).

Macrophage activation and BCM cytotoxicity

In the phagocytic activity assay, Student's *t*-test was performed to determine the difference between the absorbance resulting from the association of macrophages with cellulose, and the control group (macrophages in the presence of 0.2% DMSO in RPMI 1640 medium). In the presence of the BCM, macrophage activity was significantly increased (Fig. 9).

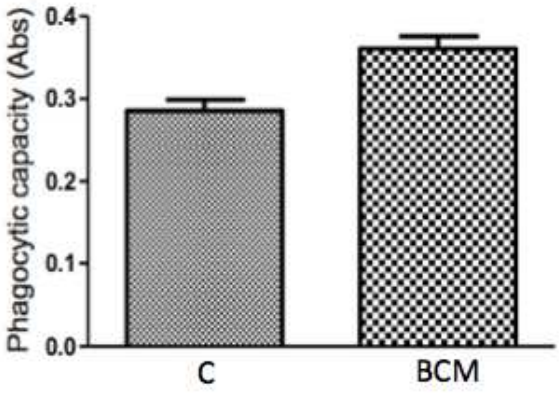

364
365 **Figure 9.** Zymosan particle phagocytosis by macrophages in the presence of the BCM. The graph represents the
366 mean ± standard error of the mean of three independent experiments performed in triplicate (control: mean 0.28567,
367 standard deviation 0.03161; BCM: mean 0.36100, standard deviation 0.03474). ABS: absorbance; C: control; BCM:
368 bacterial cellulosic membrane; *p < 0.05.
369

370 The colorimetric reading of NO release showed that the levels remained at a non-cytotoxic
371 concentration for the cells in the presence of the BCM (Fig. 10). The difference in NO release
372 between the control and BCM was statistically significant at $p < 0.05$ (p-value 0.0184, $t_{0.05}$-
373 critical: 2.6252), as was that between LPS and BCM (p-value: 0.0001; $t_{0.05}$-critical: 11.1963).

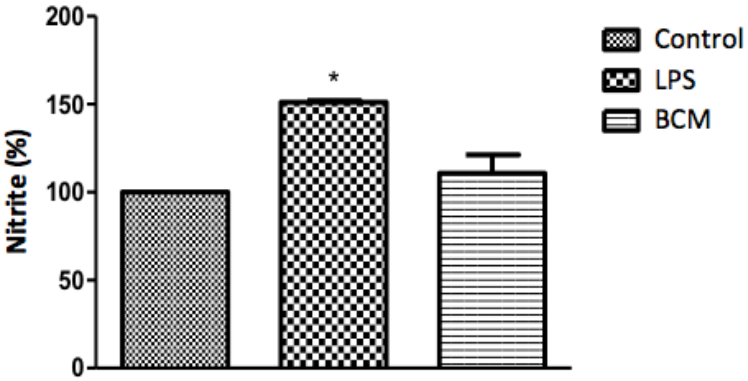

374
375 **Figure 10.** Colorimetric nitrite dosage produced by macrophages treated with lipopolysaccharide (LPS) in the
376 presence of the BCM. The plot represents the mean ± standard error of the average of three independent experiments
377 performed in triplicate (control: mean 100.0000, standard deviation 0.0000; LPS: mean 150.8889, standard deviation
378 1.0541; BCM: mean 109.6300, standard deviation 11.0047). Student's *t*-test was performed for comparison between
379 groups and the control (0.2% dimethyl sulfoxide [DMSO] in RPMI 1640 medium). C: control; LPS:
380 lipopolysaccharide; BCM: bacterial cellulosic membrane; *p < 0.05.
381

382 The tetrazole salt (MTT), incubated with cells with full metabolic activity, showed intense
383 mitochondrial activity (Fig. 11). In this trial, the metabolism of MTT by BM-MSCs showed a
384 statistically significant difference (p-value: 0.0001; $t_{0.05}$-critical: 2.6252) but there was no

statistically significant difference (p-value: 0.0628; $t_{0.05}$-critical: 2,000) between the BCM associated with murine macrophages and with the control. In both conditions, cell viability was greater than 94% (Fig. 12).

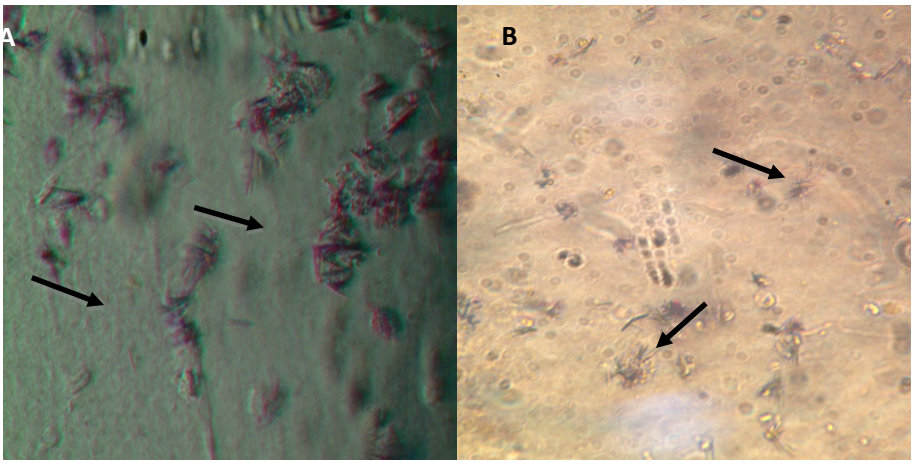

Figure 11. Formazan crystals in BCM cultured with (A) BM-MSCs, and (B) peritoneal macrophages. Increasing view 40×.

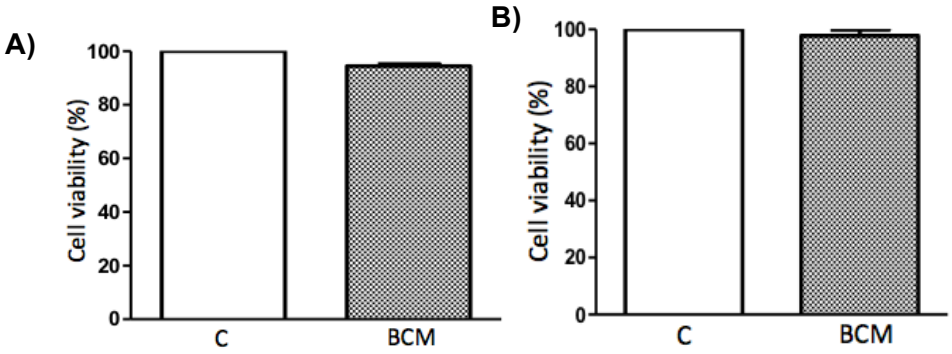

Figure 12. Effect of the BCM on BM-MSCs and mammalian peritoneal macrophage viability. (A) BM-MSC viability in the BCM (control: mean 100.0000, standard deviation 0.0000; BCM: mean 94.4533, standard deviation 1.1926), and (B) viability of murine macrophages in the BCM (control: mean 100.0000, standard deviation 0.0000; BCM: mean 97.7867, standard deviation 3.3200). The plot represents the mean ± standard error of the mean of three independent experiments performed in triplicate. Student's *t*-test was performed to compare the groups with the control (0.2% DMSO in DMEM/RPMI medium). C: control; BCM: bacterial cellulosic membrane; *p < 0.05.

Discussion

After isolation, BM-MSCs exhibited a rounded shape in culture. During the adhesion and expansion process, their morphology modified, becoming gradually fusiform, and proliferating in parallel in colonies; the exclusion of hematopoietic cells in the medium exchanges was perceptible. Similarly, Samsonraj et al. (2015) stated that MSCs adhere to favorable surfaces with rapid morphological changes, ranging from rounded to elongated shapes. According to Ikebe and

406 Suzuki (2014), adhesion to plastic is the first criterion for the characterization of MSCs. In the
407 cellular adhesion phase, physicochemical connections occur between the cells and the contact
408 surface, including ionic forces that rapidly alter cell morphology, and which are evident after 1 h
409 of culture (Pu & Komvopulos, 2014; Wang & He, 2016).

410 The organization of cells in fibroblastoid colonies has been considered by Kisiel et al.
411 (2012) as the second major characteristic of MSCs. In this experiment, colony formation was
412 evident after 2 days of primary culture, suggesting that these interactions can occur without
413 cellular differentiation, and therefore allow fibroblastoid morphology to be maintained.

414 Regarding cell viability after thawing, the lag phase was evident from day 1 to day 4 of the
415 growth curve, and the log phase occurred between days 5 and 11, with exponential mitotic
416 divisions evident mainly between days 9 and 11; a decline in the number of cell divisions
417 occurred between days 12 and 15. Seconda et al. (2015) defined the lag phase as a relatively short
418 stage characterized by onset of the release of cell proliferation factors. The exponential cell
419 growth (log) phase is the second phase, in which the growth rate and duration depend on the
420 medium used. When cellular metabolism can no longer be maintained, cells undergo apoptosis.

421 The ability to differentiate into more than one mesenchymal lineage (chondrogenic,
422 osteogenic, or adipogenic) is an important multipotentiality feature of MSCs, and is a
423 fundamental requirement for their characterization (Wuchter, Wagner & Ho 2016). According to
424 Kolf et al. (2015), the tissue formed by chondrogenic cell differentiation acquires a vibrant blue
425 color when stained with Alcian Blue; during osteogenic differentiation, it is possible to observe
426 the gradual deposition of calcium in the extracellular matrix, which is attributable to the presence
427 of osteoblasts. Alizarin Red staining showed a fairly characteristic reddish coloration, providing
428 evidence of this potential. According to Munir et al. (2017), formation of lipid vacuoles in the
429 cell cytoplasm and staining by Oil Red characterize the formation of adipocytes; during
430 adipogenic differentiation, several independent vacuoles can be found, and fuse as they expand
431 inside the cell. In this study, cell culture using specific media for differentiation into mesodermal
432 (chondrogenic, osteogenic, or adipogenic) lineages demonstrated the multipotentiality of rabbit
433 BM-MSCs.

434 Cell adhesion and proliferation largely depend on the characteristics of the biomaterial
435 surface, since interactions that occur on the surface will drive the biological responses (Chahal et
436 al., 2016; Khayyen et al., 2016). After 7 days of culture, cells showed organization in a

437 fibroblastoid format with a tendency for cell grouping. In the analysis performed at 14 days, the
438 BM-MSCs were present in colonies, and covered the BCM surface.

439 Using SEM, we verified that BM cells maintain their rounded shape on the BCM surface in
440 the first 24 h, with few biomaterial fixation bridges. A delay in BM-MSC anchoring to the BCM
441 was observed when compared to adhesion in culture plates, and this anchoring onset was evident
442 in a few hours. According to Silveira et al. (2016), the three-dimensional structure of BCM
443 nanofibers exhibits an arrangement similar to that of the collagen fibers of the extracellular
444 matrix, and a surface with different pores can provide variable times for cell adhesion to the
445 biomaterial.

446 BM-MSC anchoring and proliferation on the BCM were evident on day 7 of culture with
447 grouped cells, and several cytoplasmic projections were evident in the BCM. On the 14th day of
448 culture, fixation of the BM-MSCs occurred by interaction with the biomaterial. Consistent with
449 the studies of Alberti and Xu (2016) and Santana et al. (2014), the presence of cytoplasmic
450 projections and normal cell morphology are factors that confirm cytocompatibility between the
451 BCM scaffold and cells.

452 Equilibrium in immune system cell activation also reflects a tissue's regenerative quality.
453 In the presence of the BCM, the macrophages presented a statistically significant increase (p-
454 value 0.0002; $t_{0.05}$-critical: 4.8118) in their activity compared with the control group. Qiu et al.
455 (2016) clarified that maintaining the scaffold intact during the period of adhesion and cell
456 proliferation is important for the regenerative process and the architecture of the tissue to be
457 repaired. The implanted biomaterial should gradually biodegrade to give rise to newly formed
458 tissue without exacerbating an inflammatory response that compromises the repair quality. Thus,
459 the adequate inflammatory response of the host in specific situations makes the biomaterial
460 compatible with its use.

461 The ability of bacterial cellulose to be degraded has not yet been fully elucidated. In animal
462 and human tissues, it is considered limited due to the absence of hydrolases that rupture the ß
463 (1,4) binding of the cellulose chain, which is responsible for the solubility of the biomaterial
464 (Oliveira, Rambo & Porto, 2013). Although the idea of a completely degradable scaffold is
465 interesting from the point of view of tissue engineering, there remain difficulties with materials
466 that exhibit this property, since the timing of degradation and tissue repair combined with the
467 mechanical properties acquired by the newly formed tissue have led researchers to believe that a

468 material with a low rate of degradation may respond better when the scarring process requires
469 more time-consuming conditions (Bhattacharjee et al., 2015).

470 After inflammation, macrophages release NO as a way to eliminate pathogens. In addition,
471 NO is known as an inflammatory response mediator, inhibiting or inducing inflammation
472 according to the concentration of NO released (Taraballi et al., 2016). The colorimetric nitrite
473 dosage produced by macrophages in the presence of the BCM showed a non-cytotoxic
474 concentration, approaching the value obtained in the control group.

475 The MTT assay is a method to assess cell viability widely used to evaluate the metabolism
476 of MTT in the mitochondria of viable cells when incubated with cells with full metabolic activity
477 crossing the plasma membrane, and which, when coming in contact with the superoxide
478 produced by mitochondrial activity, is reduced by succinate dehydrogenase present in MTT-
479 formazan-containing mitochondria. The crystals formed are insoluble in water; however, they are
480 solubilized in DMSO medium, and show violet coloration. Thus, cell viability is directly
481 proportional to the intensity of staining (Toh, Yap & Lim, 2015). According to Li, Zhou, and Xu
482 (2015), a material is considered non-cytotoxic and biocompatible when cell viability is greater
483 than 70%. In this study, the MTT assay presented intense violet staining, showing that the BCM
484 does not produce a toxic effect on the cells; 94% cellular viability is considerably favorable for
485 non-interference of cellular activity.

486

487 **Conclusion**

488 The expansion and cellular integration of biomaterials depends greatly on the quality and
489 suitability of the biomaterial surface. The BCM allowed the adhesion, expansion, and
490 biointegration of BM-MSCs, and the cytotoxicity and toxicity of the BCM were low enough to
491 maintain considerable viability in cell culture. Macrophage activation and the rate of BCM
492 degradation make the BCM an ideal biomaterial for slow healing processes in which
493 reconstructed tissues require a scaffold with longer durability.

494 Considering the interaction demonstrated between BM-MSCs and the BCM, it can be
495 stated that the BCM is a promising biomaterial in tissue engineering and regenerative medicine.
496 However, it will be necessary to test the behavior of BCM implants *in vivo*.

497 **Acknowledgments**

We thank the National Council for Scientific and Technological Development – CNPq (Process: 427626 /2016-1) for financial support.

The Integrated Nucleus of Morphology and Stem Cell Research (NUPCelt), Interdisciplinary Laboratory of Advanced Materials (LIMAV), Advanced Microscopy Multiuser Laboratory (LMMA) and Antileishmania Activity Laboratoy (LAA) from the Federal University of Piauí – UFPI as well as the Laboratory of Toxicological Research – LAPETOX of University of Sorocaba – UNISO.

The protocol was approved by the Committee on Ethics in the animals use of the Federal University of Piauí (CEUA-UFPI, Permit Number 268/16).

ADDITONAL INFORMATION AND DECLARATIONS

Funding

This work had the financial support of the National Council of Scientific and Technological Development – CNPq (Process: 427626/2016-1).

Grant Disclosures

The following grant informations was disclosed by the authors:

CNPq (Process: 427626/2016-1)

Integrated Nucleus of Morphology and Stem Cell Research – NUPCelt.

National Council of Scientific and Technological Development – CNPq (Process: 427626/2016-1

Competing Interests

The authors declare there are no competing interests.

Authors contributions

- Marcello Silva performed the experiments, analyzed the data, wrote the document, prepared the figures and revised the manuscript drafts.
- Yulla Leite, Camila Carvalho, Matheus Feitosa contributed with tools and figures analysis.
- Angela Jozala prepared and yielded the bacterial cellulosic membrane.
- Acelina Martins de Carvalho, Maria Angelica Miglino conceived and designed the experiments, revised manuscript.

Ethics Committee

528 The study was carried out in accordance with the recommendations of the Guide for the
529 Laboratory Animals Care and Use of the National Institute of Health. The protocol was approved
530 by the Ethics Committee on Animal Use of the Federal University of Piauí (CEUA-UFPI, permit
531 number: 268/16).
532

533 **REFERENCES**

534

535 **Abbott R, Kaplan D. 2016.** Engineering Biomaterials for Enhanced Tissue Regeneration, *Current Stem*
536 *Cell Reports*, **22(2)**:140-146. DOI: 10.1007/s40778-016-0039-3.

537 **Achatz F, Kujat R, Pfeifer C, Koch M, Nerlich M, Angele P, Zellner J. 2016.** *In Vitro* Testing of
538 *Scaffolds* for Mesenchymal Stem Cell-Based Meniscus Tissue Engineering—Introducing a New
539 Biocompatibility Scoring System, *Materials*, **9(4)**:1-14 DOI: 10.3390/ma9040276.

540 **Agatha H. Kisiel DVM, Laurie A, Mcduffee DVM, Masaoud E, Bailey TR, Gonzalez BPE, Fong-**
541 **Nino R. 2012**. Isolation, characterization, and *in vitro* proliferation of canine mesenchymal stem cells
542 derived from bone marrow, adipose tissue, muscle, and periosteum, *American Journal of Veterinary*,
543 **73(8)**:1305-1317 DOI 10.2460/ajvr.73.8.1305.

544 **Argôlo Neto NM, Feitosa MLT, Sousa SS, Fernandes PB, Pessoa GT, Bezerra DO, Almeida HM,**
545 **Carvalho YKP, Rocha AR, Silva LMC, Carvalho MAM. 2016.** Isolation, Expansion, Differentiation
546 and Growth Kinetics Essay in Mesenchymal Stem Cells Culture from the Bone Marrow of Collared
547 Peccaries (Tayassu tajacu). *Acta Scientiae Veterinariae*, **44(1341)**: 1-11.

548 **Alberti KA, Xu Q. 2016.** Biocompatibility and degradation of tendon-derived *scaffolds*, *Regenerative*
549 *biomaterials*, **1(1)**:1-11 DOI 10.1093/rb/rbv023.

550 **Barud HGO, Barud HS, Cacicchioli M, Amaral TS, Oliveira Junior OB, Santos DM, Petersen**
551 **ALOA, Celes F, Borges VM, Oliveira CI, Oliveira PF, Furtado RA, Tavares DC, Ribeiro SJL. 2015.**
552 Preparation and characterization of a bacterial cellulose/silk fibroinsponge scaffold for tissue regeneration.
553 *Carbohydrate Polymers*. **128**: 41-51 DOI 10.1016/j.carbpol.2015.04.007.

554 **Bhattacharjee M, Coburn J, Centolo M, Murab S, Barbero A, Kaplan DL, Martin I, Ghosh S. 2015.**
555 Tissue engineering strategies to study cartilage development degeneration and regeneration. *Advanced*
556 *Drug Delivery Reviews*. **85**:107-122.

557 **Blanquer SBG, Grijpma DW, Poot AA. 2015.** Delivery systems for the treatment of degenerative
558 intervertebral discs. *Advanced Drug Reviews*. **84**:172-187 DOI 10.1016/j.addr.2014.10.024.

559 **Castellanos AM, Balkan W, DiFede DL, Hare JM. 2016.** Cell infection site influences the human
560 mesenchymal stem cell therapy effectiveness for left ventricular dysfunction in ischemic cardiomyopathy.
561 *Circulation*. **123(1)**:A192102 DOI 10.1161/ CIRCULATIONAHA.116.024610.

562 **Chahal S, Hussain FSJ, Kumar A, Rasad MSBA, Yusoff MM. 2016.** Fabrication, characterization and
563 *in vitro* biocompatibility of electrospun hydroxyethyl cellulose/poly (vinyl) alcohol nanofibrouscomposite
564 biomaterial for bone tissue engineering, *Chemical Engineering Science*, **144(22)**:17-29 DOI
565 10.1016/j.ces.2015.12.030.

566 **Cruz IBM, SEVERO AL, Azzolin VF, Garcia LFM, Kuhn A, Lech O. 2016.** Potencial regenerativo do
567 tecido cartilaginoso por células-tronco mesenquimais: atualização, limitações e desafios. *Revista*
568 *Brasileira de Ortopedia*. 1-9 DOI 10.1016/j.rbo.2016.02.007.

DiMarino AM, Caplan AI & Bonfield TL. 2013. Mesenchymal stem cells in tissue repair. *Frontier in Immunology*, **4**:1-9 DOI 10.3389/fimmu.2013.00201.

Emmet TM, Amos M, Daniel KJ, John GP, O'Brien FJ. 2016. An Endochondral Ossification-Based Approach to Bone Repair: Chondrogenically Primed Mesenchymal Stem Cell-Laden Scaffolds Support Greater Repair of Critical-Sized Cranial Defects Than Osteogenically Stimulated Constructs In Vivo. *Tissue Engieering Part A*. **22(5-6)**: 556-567 DOI 10.1089/ten.tea.2015.0457.

Fávaro RC, Arruda AO, Vialle LR, Vialle EN. 2016. Influência da terapia celular mononuclear sobre a degeneração discal em coelhos. Revista Brasileira de Ortopedia. **1(9)**. DOI 10.1016/j.rbo.2016.03.007.

Fu L, Zhang J, Yang G. 2013. Present status and applications of bacterial cellulose-based materials for skin tissue repair. *Carbohydrate Polymers*. **92**:1431-1442.

Ikebe C, Suzuki K. 2014. Mesenchymal Stem Cells for Regenerative Therapy: optimization of Cell Preparation Protocols, *Biomed Research International*. **1(1)**:1-11 DOI 10.1155/2014/951512.

Jozala AF, Pértile RAN, Santos CA, Santos-Ebinuma VC, Seckler MM, Gama FM, Pessoa Junior A. 2015. Bacterial cellulose production by *Gluconacetobacter xylinus* by employing alternative culture media. *Applied Microbiology and Biotechnology*. **99(3)**: 1181-1190 DOI 10.1007/s00253-014-6232-3.

Kaplan JM, Youd ME, Lodie TA. 2011. Immunomodulatory activity of mesenchymal stem cells. *Current Stem Cell Research & Therapy.* **6(4)**:297-316 DOI 10.2174/157488811797904353.

Kobolak J, Dinnyes A, Memic A, Khademhosseini A, Mobasheri A. 2016. Mesenchymal stem cells: Identification, phenotypic characterization, biological properties and potential for regenerative medicine through biomaterial micro-engineering of their niche. *Methods*. **99**: 62-68. DOI 10.1016/j.ymeth.2015.09.016.

Khayyeri H, Longo G, Gustafsson A, Isaksson H. 2016. Comparison of structural anisotropic soft tissue models for simulating Achilles tendon tensile behavior. *Journal of the mechanical behavior of biomedical materials*, **6(1)**:431-443 DOI /10.1016/j.jmbbm.2016.04.007.

Kim M, Kim G. 2015. 3D multi-layered fibrous cellulose structure using an electrohydrodynamic process for tissue engineering. *Journal of Colloid and Interface Science*. **457**:180-187. DOI 10.1016/j.jcis.2015.07.007.

Kolf CM, Song L, Helm J, Tuan RS. 2015. "Nascent osteoblast matrix inhibits osteogenesis of human mesenchymal stem cells *in vitro*". *Stem Cell research & Therapy*, **22(6)**:1-16 DOI 10.1186/s13287-015-0223-x.

Langer R, Vacanti J. 2016. Advanced in tissue engineering, *Journal of Pediatric Surgery,* **1(51)**:8-12 DOI 10.1016/j.jpedsurg. 2015.10.022.

Li W, Zhou J, Xu Y. 2015. Study of the in vitro cytotoxicity testing of medical devices (Review). *Biomedical Reports*. **3**: 617-620 DOI 10.3892/br.2015.481.

Li X, Yuan Z, Wei X, LI H, Zhao G, Miao J, Wu D, Liu B, Cao S, An D, Ma W, Zhang H, Wang W, Wang Q, Gu H. 2016. Application potencial of bone marrow mesenchymal stem cell (BMSCs) based tissue-engineering for spinal cord defect repair in rat fetuses with spina bifida aperta, *Tissue engineering constructs and cell substrates*, **27(4)**: 1-11 DOI 10.1007/s10856-016-5684-7.

Lima FMT, Pinto FCM, Costa BLSA, Silva JGM, Campos Júnior O, Aguiar JLA. 2017. Biocompatible bacterial cellulose membrane in dural defect repair of rat. *Journal of Materials Science: Materials in Medicine*. 28-37. DOI 10.1007/s10856-016-5828-9.

Lin WC, Lien CC, Yeh HJ, Yu CM, Hsu SH. 2013. Bacterial cellulose and bacterial cellulose-chitosan membranes for wound dressing applications. *Carbohydrate Polymers*. **94**: 603-611 DOI 10.1016/j.carbpol.2013.01.076.

Munir H, Ward LSC, Sheriff L, Kemble S, Nayar S, Barone F, Nash GB, McGettrick HM. 2017. Adipogenic differentiation of mesenquimal stem cells afters their immunomodulatory properties in a tissue-specifc manner. *Stem Cells*. DOI 10.1002/stem.2622.

Oliveira VA, Rambo CR, Porto LM. 2013. Produção e degradação in vitro de estruturas tubulares de celulose bacteriana. *Polimeros*. DOI 10.4322/polimeros.2013.041.

Park S-B, Lih E, Park K-S, Joung YK, Han DK. 2017. Biopolymer-based functional composites for medical applications. *Progress in Polymer Science*. 77-105. DOI 10.1016/j.progpolymsci.2016.12.003.

Peach MS, Ramos DM, James R, Morozowich NL, Mazzocca AD, Doty SB, Allcock HR, Kumbar SG, Laurencin CT. 2017. Engineered stem cell niche matrices for rotador cuff tendo regenerative engineering. *Plos One*. 1-19. DOI 10.1371/journal.pone.0174789.

Pires A, Bierhalz A, Moraes A. 2015. Biomateriais: tipos, aplicações e mercado, *Química nova*, **38(7)**: 957-971 DOI 10.5935/0100-4042.20150094.

PU J, Komvopoulos K. 2014. Mechanical properties of electrospun bilayer fibrous membranes as potential *scaffolds* for tissue engineering, *Acta Biomaterialia*, 10(1):2718-2726. DOI 10.1016/j.actbio.2013.12.060.

Qiu Y, Qiu L, Cui J, Wei Q. 2016. Bacterial cellulose and bacterial cellulose-vaccarin membranes for wound healing. *Materials Science and Engineering C*. **59**:303-309.

Rajwade JM, Paknikar KM, Kumbhar JV. 2015. Applications of bacterial cellulose and itd composites in biomedicine. *Appl Microbiol Biotechnol*. **99**:2491-2511. DOI 10.1007/s00253-015-6426-3.

Samsonraj RM, Rai B, Sathiyanathan P, Puan Kj,Rötzschke O, Hui JH, Raghunath M, Stanton LW, Nurcombe V, Cool SM. 2015. Establishing Criteria for Human Mesenchymal Stem Cell Potency, *Translational and Clinical Research*, **1(1)**:1878-1891 DOI 10.1002/stem.1982.

Santana CC, Nóbrega Neto PI, Sá MJC. 2014. Utilização do filme de quitosana na reparação de tendão em coelhos. *Arquivo brasileiro de medicina veterinária e zootecnia*, **66(4)**:995-1002 DOI 10.1590/1678-6521.

Schnitzler AC, Verma A, Kehoe DE, Jing D, Murrell JR, Der KA, Aysola M, Rapiejko PJ, Punreddy S, Rook MS. 2016. Bioprocessing of human mesenchymal stem/stromal cells for therapeutic use: Current technologies and challenges. *Biochemical Engineering Journal*. **108**:3-13.

Secunda R, Vennila R, Mohanashankar AM, Rajasundari S, Surendran R. 2015. Isolation, expansion and characterisation of mesenchymal stem cells from human bone marrow, adipose tissue, umbilical cord blood and matrix: a comparative study, *Cytotechnology*, **67(5)**:793-807 DOI: 10.1007/s10616-014-9718-z.

Silveira RK, Coelho ARB, Pinto FCM, Albuquerque AV, Filho DAM, Aguiar, JLA. 2016. Bioprosthetic mesh of bacterial cellulose. *Materials in Medicine*, **27(8)**:1-9 DOI: 10.1007/s10856-016-5744-z.

Soheilmoghaddam M, Sharifzadeh G, Pour RH, Wahit MU, Whye WT, Lee XY. 2014. Regenerated cellulose/ β-cyclodextrin scaffold prepared using ionic liquid. *Material Letters*. **135**: 210-2013 DOI: 10.1016/j.matlet.2014.07.169.

Souza AC, Alves MMM, Brito LM, Oliveira LGC, Sobrinho-Júnior EPC, Costa ICG, Freitas SDL, Rodrigues KAF, Chaves MH, Arcanjo DDR, Carvalho AA. 2017. *Platonia insignis* Mart., a Brazilian Amazonian Plant: The Stem Barks Extract and Its Main Constituent Lupol Expert Antileishimanial Effects Involving Macrophages Activation. *Evidence-Based Complementary and Alternative Medicine.* **2017**: 1-12 DOI: 10.1155/2017/3126458

Squillaro T, Peluso G, Galderisi. 2016. Clinical trials with mesenchymal stem cells: an update. *Cell Transplatation*, **25**:829-848 DOI:10.3727/096368915X689622.

Sundaram J, Pant J, Goudie MJ, Mani S, Handa H. 2016. Antimicrobial and Physicochemical Characterization of Biodegradable, Nitric Oxide-Releasing Nanocellulose–Chitosan Packaging Membranes. *Journal of Agricultural and Food Chemistry*. 64(25): 5260-5266 DOI: 10.1021/acs.jafc.6b01936.

Taraballi F, Corradetti B, Minardi S, Powel S, Cabrera F, Van Eps JL, Weiner BK, Tasciotti E. 2016. Biomimetic collagenous scaffold to tune inflammation by targeting macrophages. Journal of Tissue Engeneering. **7**:1-13 DOI: 10.1177/204173141524667.

Toh WS, Yap AUJ, Lim SY. 2015. In vitro biocompatibility of contemporary bulk-fill composites. *Operative Dentistry*. **40(6)**:644-652. DOI 10.2341/15-059-L.

Urbina L, Algar I, García-Astrain C, Gabilondo N, González A, Corcuera MA, Eceiza A, Retegi A. 2016. *Journal of Applied Polymer*. 1-10 DOI: 10.1002/APP.43669.

Wang S, Qu X, Zhao R.C. 2012. Clinical applications of mesenchymal stem cells. *Journal of Hematology & Oncology*, **19(5)**:1-9.

Wang W, He J, Feng B, Zhang Z, Zhou G, Cao Y, Fu W, Liu W. 2016. Aligned nanofibers direct human dermal fibroblasts to tenogenic phenotype *in vitro* and enhance tendon regeneration *in vivo*, *Nanomedicine*, **11(9)**:1055-1072 DOI: 10.2217/nnm.16.24.

673 **Wei X, Yang X, Han Z, Qu F, Shao L, Shi Y. 2013.** Mesenchymal stem cells: a new trend for cell
674 therapy, *Acta Pharmacologica Sinica*, **34(6)**:747-754 DOI: 10.1038/aps.2013.50.

675 **Weinstein-Oppenheimer CR, Brown DI, Coloma R, Morales P, Reyna-Jeldes M, Diaz MJ, Sánchez**
676 **E, Acevedo CA. 2017**. Design of a hybrid biomaterial for tissue engineering: Biopolymer-scaffold
677 integrated with an autologous hydrogel carrying mesenchymal stem-cells. *Materials Science and*
678 *Engineering: C*. **79**; 821-830 DOI 10.1016/j.msec.2017.05.116.

679 **Wuchter P, wagner W, Ho A.D. 2016.** Mesenchymal Stromal Cells (MSC). IN: Regenerative Medicine
680 – From protocol to Paciente**.** 3 ed. Switzerland: Springer.

681 **Xi J, Yan X, Zhou J, Yue W, Pei X. 2013.** Mesenchymal stem cells in tissue repairing and regeneration:
682 Progress and future. *Burns & Trauma*, **1(1)**:13-20.

683 **Zhao Q, Ren H, Han Z. 2016.** Mesenchymal stem cells: Immunomodulatory capability and clinical
684 potencial in imune diseases. *Journal of Cellular Immunotherapy*, **2**:3-20 DOI:
685 10.1016/j.jocit.2014.12.001.

686 **Zulkifli FH, Hussain FSJ, Rasad MSA, Yusoff MM. 2014.** Nanostructure materials from hydroxyethyl
687 cellulose for skin tissue engineering. *Carbohydrate Polymers*. **144**:238-245 DOI:
688 10.1016/j.carbpol.2014.08.019.